Quantum-chemical modeling of the hydrocarbon transformations in acid zeolite catalysts

Topics in Catalysis 9 (1999) 191–205

Quantum-chemical modeling of the hydrocarbon transformations in acid zeolite catalysts

M.V. Frash and R.A. van Santen

Eindhoven University of Technology, PO Box 513, 5600 MB Eindhoven, The Netherlands

Results of quantum-chemical modeling of a number of elementary steps involved in the acid zeolite-catalyzed conversion of hydrocarbons are collected together and compared. The elementary steps considered are protolytic cracking, protolytic dehydrogenation, hydride transfer, skeletal isomerization, and β-scission. The hydrocarbon parts of transition states (TS) for these steps represent carbocations specific for each reaction. Geometry parameters of the TS and activation energies depend on the relative stability of these carbocations. The reactions considered can proceed via several alternative routes dependent on the species involved and on the details of the interaction of the hydrocarbon portion of the activated complex with the zeolite oxygen atoms. Variation of the acid strength of zeolite cluster models can be employed for studies of the acid strength sensitivity of the activation energies and other quantities of interest as well as for extrapolation of these quantities computed on small clusters towards zeolitic values.

Keywords: catalytic cracking, hydrocarbon conversion, acid zeolite catalysts, quantum chemistry, transition states, carbenium and carbonium ions

1. Introduction

Conversion of hydrocarbons by zeolite acid catalysts is very important for the modern oil and chemical industry [1–3]. Here we present a state of the art review of quantum-chemical studies on a few Brønsted acid catalyzed hydrocarbon conversion reactions. A great number of experimental studies as well as theoretical work has provided a detailed mechanistic understanding of such reactions. Initial elementary reaction steps occurring on Brønsted acid sites (BAS) are chemisorption of olefins (1), protolytic cracking of paraffins (2), and protolytic dehydrogenation of paraffins (3):

$$R^{=} + H^{+}_{ads} \rightarrow R^{+}_{ads} \quad (1)$$

$$R_1\text{–}R_2 + H^{+}_{ads} \rightarrow R^{+}_{1ads} + R_2\text{–}H \quad (2)$$

$$R_1\text{–}H + H^{+}_{ads} \rightarrow R^{+}_{1ads} + H_2 \quad (3)$$

The adsorbed "carbenium ions" R^{+}_{ads} correspond to surface alkoxy groups [4]. These groups undergo further transformations such as skeletal isomerization (4), β-scission (5) and alkylation (6):

$$R_1R_2CH\text{–}R_3CH^{+}_{ads} \rightarrow R_2R_3CH\text{–}R_1CH^{+}_{ads} \quad (4)$$

$$R\text{–}CH_2\text{–}(CH_3)CH^{+}_{ads} \rightarrow R^{+}_{ads} + H_2C{=}CH\text{–}CH_3 \quad (5)$$

$$R^{+}_{ads} + H_2C{=}CH\text{–}CH_3 \rightarrow R\text{–}CH_2\text{–}(CH_3)CH^{+}_{ads} \quad (6)$$

as well as aromatization and coke formation. New surface alkoxy groups formed in the reactions (4)–(6) can yield olefins regenerating free Brønsted acid sites (7), or enter the hydride transfer reaction, thus involving new hydrocarbon molecules into the chain catalytic process (8):

$$R^{+}_{ads} \rightarrow H^{+}_{ads} + R^{=} \quad (7)$$

$$R^{+}_{1ads} + R_2\text{–}H \rightarrow R^{+}_{2\,ads} + R_1\text{–}H \quad (8)$$

Extensive quantum-chemical studies on the reactions of H–D exchange [5–10], olefin chemisorption–desorption [11–13], and transformations of methanol [14–19] have already been reported. Most of these studies were performed in the frame of the cluster approach [20–24]. New promising techniques such as combined MM/MO approach [25–28], embedding technique [29,30] and plane wave DFT [19,31,32] are now introduced in modeling of heterogeneous catalysis. These techniques are able to account for steric effects and long-range Coulomb fields that are neglected in the cluster calculations. However, so far relatively few results are obtained with these new methods.

A large number of hydrocarbon elementary reactions was studied by quantum-chemical methods in the work of Rigby et al. [33]. Transition states for almost all reaction types (1)–(8) of various hydrocarbons and surface alkoxy groups were located and the corresponding activation energies computed. The calculations indicated that alkoxy groups covalently bound to one of the bridging oxygen atoms of the acid site are stable intermediates, whereas transition states resemble carbocations, in agreement with the finding of Kazansky [4]. It was also found that there is almost no energy ordering according to the primary, secondary or tertiary nature of surface alkoxy groups. The success of the carbocation model predictions of preferred reaction pathways is due to variation in the reaction barriers with the nature of the initial and/or final alkoxy. A number of other quantum-chemical works addressed more limited sets of reactions, although in some cases at more precise levels of theory and without symmetry constraints used in [33]. Results of these works agree well with the results of Rigby et al. [33] in the predicted nature of transition states and in the calculated activation energy differences, whereas details of the reaction route and the absolute

values of activation energies may be significantly different.

The aim of the present review is to collect together and compare published results of the quantum-chemical modelling of the following elementary reactions involving hydrocarbons and surface alkoxy groups: (i) protolytic cracking of paraffins (equation (2)); (ii) protolytic dehydrogenation of paraffins (equation (3)); (iii) hydride transfer (equation (8)); (iv) skeletal isomerization (equation (4)); (v) β-scission (equation (5)) and alkylation (equation (6)). We consider reaction routes, transition state geometries and activation energies, and discuss dependence of geometry and energy characteristics on the type of species undergoing the reaction and on the model and calculation level used. Besides this, use of the cluster acid strength variations in modeling will be discussed.

2. Methods of calculations

2.1. Cluster models, quantum-chemical methods, and geometry constraints

All the reported calculations on the reactions under consideration were performed in the frame of the cluster approach [20–24]. The zeolite Brønsted acid sites were modeled by one of the following molecular clusters: H_3Si–(OH)–$Al(OH)_2$–O–SiH_3, H_3Si–(OH)–AlH_2–O–SiH_3, H–(OH)–$Al(OH)_2$–O–H, or H–(OH)–AlH_2–O–H. Calculations with these clusters are sufficient to describe chemical rearrangements that occur locally on the acid sites. Use of larger clusters, e.g., H_3Si–(OH)–$Al(O–SiH_3)_3$ [34] leads to potentially more accurate results but significantly increases the computational requirements; this is particularly important when transition states are to be sought. The silicon-containing clusters H_3Si–(OH)–$Al(OH)_2$–O–SiH_3 and H_3Si–(OH)–AlH_2–O–SiH_3 are more realistic and have deprotonation energies that are closer to the real zeolite values than those of the silicon-free clusters H–(OH)–$Al(OH)_2$–O–H, or H–(OH)–AlH_2–O–H (see section 4). The latter clusters are, however, still useful when computational requirements are to be minimized or when dependence of the quantities of interest on the cluster deprotonation energy is to be studied. Amongst the two silicon-containing clusters, H_3Si–(OH)–$Al(OH)_2$–O–SiH_3 seems at the first glance to be better since it has a more correct chemical surrounding of aluminum and costs in computations only slightly more than H_3Si–(OH)–AlH_2–O–SiH_3. However, calculation results [8,9] indicate that replacement of terminating hydroxyls with terminating hydrogens has only a small effect on the computed quantities of interest. Moreover, the H_3Si–(OH)–$Al(OH)_2$–O–SiH_3 cluster sometimes causes computational problems when the substrate molecule trends to interact with the more basic oxygens of the Al–O–H groups while the more chemically appropriate oxygens of the Al–O–Si groups are left unengaged. This makes it more convenient to use the H_3Si–(OH)–AlH_2–O–SiH_3 cluster. Dependence of the zeolite cluster deprotonation energy on the cluster size and the Si/Al ratio has been systematically studied [35,36]. Unfortunately, there were no similar detailed studies performed so far for the activation energies of the elementary steps of hydrocarbon conversion being considered here. This issue is of large interest but will require a lot of computational resources particularly for the transition states location.

The methods most commonly used in quantum-chemical studies of the zeolite catalysis are the Hartree–Fock method (HF) [37], the Møller–Plesset second order perturbation method (MP2) [37] and a number of the density functional methods (DFT) [38]. The basis sets applied vary from the very small 3-21G [37] to the split-valence, double-zeta, or triple-zeta basis sets with polarization and diffuse functions. Differences in the results due to different methods of calculation applied for the same reaction and the same hydrocarbon are of significant interest. The following trends can be observed based on the reported data. The calculated activation energies strongly depend on the level of the final energy calculations and less on the level of the geometry optimization [39–41]. Therefore it is useful to perform the geometry optimization at a lower level (HF or DFT with a basis set of a moderate size, e.g., 6-31G* [37]) followed by the single point final energy calculation at a higher level (correlated MP2 or DFT with a larger basis set, e.g., 6-31++G**). In most cases the single point activation energies found at the correlated MP2 and DFT levels are lower and closer to the experimental data than the HF values (the β-scission reaction discussed in the section 3.5 is an exception with the MP2 values slightly higher than HF). Geometry optimization at the HF and DFT (B3LYP) level gave similar structures and reaction routes in several cases [39,40]. However, in case of β-scission the reaction routes found at the B3LYP and HF levels are different [41] and the HF route is in better agreement with conventional wisdom than the B3LYP one. On the other hand, geometry optimization applying the DFT methods is found to be much better than HF for free carbocations [42,43]. Therefore it is sensible to perform calculations with the HF and DFT geometry optimization in parallel and to compare the results.

Geometry constraints were used in some works in order to accelerate computations or model special effects. For example, imposing the planar symmetry greatly accelerates calculations but significantly affects the computed quantities of interest [33,44]. In contrast, if only five atoms of the cluster (one Al, two O and two Si) are fixed in one plane while positions of other atoms are fully optimized [44,45], then the calculations are somewhat accelerated and the obtained activation energies are almost unaffected. The only disadvantage of this constraint consists in possible additional imaginary vibrational modes of the TS that make the analysis of modes more difficult. Constraining the cluster terminal Si–H bonds at values different from the equilibrium distance is a tool for varying the cluster acid strength in calculations [5,6,9,33,46].

2.2. Location and verification of transition states

Computation of the most important kinetic parameter of a reaction – activation energy – requires location of the transition state (TS). Usually location of a TS requires significantly more both computing time and researcher's efforts than location of a local minimum (LM) structure containing the same number of atoms and basis functions. A general discussion on the TS search can be found elsewhere [37,47]. However, several tools will be mentioned here:

(1) Choice of the chemically sensible initial geometry for the TS search. Use of the TS geometries from a lower computation level and/or a similar but smaller system is an option.

(2) Use of the rationally constructed Z-matrix, avoiding the cycle effects and nearly linearly dependent variables. Geometry optimization in redundant internal coordinates [48] implemented in the Gaussian94 program package is a convenient alternative to the Z-matrix optimization. However, in the case of the TS search in redundant coordinates one has to make sure that the program detects the elongated bonds being formed or broken in the reaction.

(3) The analytically computed hessian is very useful for the TS search. Less efficient but computationally less demanding is the use of the hessian computed at a lower level.

(4) Stepwise optimization of geometry. Simultaneous optimization of all the geometry parameters is more convenient since less or no restarts are necessary. However, often it does not work for the TS search, e.g., because soft modes chemically not associated with the reaction coordinate become involved after several steps due to the hessian update scheme used. This problem can be solved with splitting the set of variables into two groups: the first (small) group of variables contributing essentially to the reaction coordinate, and the second group of variables that almost do not contribute. Then one optimizes these two groups separately (the first group as a TS while the second group as a local minimum) until gradients are small, after that the whole set of variables is optimized simultaneously.

Once a transition state is located, it has to be proven that this is indeed a TS and that it connects the correct reagents and products. There are three main criteria:

(1) Usually the proper TS geometry is chemically sensible, in particular the bonds being broken or formed in the reaction have larger lengths in the TS than in the initial or final structures.

(2) Analysis of the vibration modes provides a more objective assessment of the structure obtained. The TS computed without any symmetry constraints must have one and only one imaginary mode. This mode should be associated with the reaction coordinate and composed mainly of the displacements of the atoms whose chemical surrounding is changed in the reaction. Note that if geometry constraints were applied, then the TS structure can contain more than one imaginary mode (one associated with the reaction coordinate while others caused by the geometry constraints) and this makes the analysis more difficult.

(3) The most reliable method for finding the reagents and products connected by a given TS is the intrinsic reaction coordinate method (IRC) [49], however, rarely used for large systems because it is extremely time-consuming. The faster and more usual method is "geometry relaxation": one slightly distorts the TS geometry in both directions of the negative eigenvector and performs the local minimum optimization of the two distorted structures to reach the initial and final states involved.

3. Results of calculations

3.1. Protolytic cracking of paraffins

Protolytic cracking is one of the elementary steps responsible for the initiation of chain catalytic transformations of paraffins in zeolites. The reaction consists in protolytic cleavage of a C–C bond of paraffin by a proton transferred from the zeolite Brønsted acid site. The proton attaches to one of the carbon atoms leading to formation of a smaller paraffin, whereas the second hydrocarbon residue either collapses to a surface oxygen or forms olefin. Quantum chemical calculations on protolytic cracking of ethane [9,33,50–52], propane [33], n-butane [53,54], isobutane [51], and n-hexane [53] were reported. All the results obtained are consistent that the reaction proceeds via a transition state with a nonclassical three-centered bond C(1)–C(2)–H(1), the H(1) hydrogen still bound to a zeolite oxygen O(1) (see table 1). An example of isobutane protolytic cracking is shown in figure 1 (C(2) carbon binds to H(1) after decomposition of the TS, while C(1) binds to the zeolite surface).

A relatively short distance between the C(1) carbon atom and a surface oxygen O(2) (2.2–2.7 Å) is specific for the TS for *ethane* protolytic cracking as found at different levels of theory [9,50–52] (see table 1). This is not the case for cracking of larger n-paraffins [33,54] and of isobutane [51] where C(1) in the TS is at a long distance from the surface oxygen atoms (3.2–3.6 Å). This reflects the higher stability of the primary and secondary carbenium-ionic fragments formed in cracking of n-butane, n-hexane, and isobutane in comparison to the methyl fragment which can be only formed in ethane cracking.

The difference in reaction routes found for cracking of C_3^+ n-paraffins and for isobutane relates to the fate of the carbenium-ionic fragment formed after the C–C bond cleavage. Our calculations [51] for the cracking of isobutane pre-

Table 1
Protolytic cracking. Geometry parameters of the transition states in Å, activation energies in kcal/mol.

Model	I	II	III	IV		V	
Paraffin	C_2H_6	C_2H_6	C_2H_6	C_2H_6	i-C_4H_{10}	n-C_4H_{10}[a]	n-C_4H_{10}[b]
C(1)–C(2)	2.064	2.196	2.252	2.168	1.859	2.13	2.31
C(2)–H(1)	1.173	1.175	1.137	1.141	1.256	1.21	1.30
C(1)–H(1)	1.586	1.373	1.471	1.479	1.321	1.35	1.26
O(1)–H(1)	1.913	2.393	2.447	2.076	1.705	2.01	2.16
C(1)–$O_{nearest}$	2.203	2.545	2.712	2.594	3.242	(3.54)[c]	(3.58)[c]
$E^{\#}$	69.8	71.4	75.5	80.3	57.5	60.8	55.4

I – Blaszkowski et al. [9] (cracking 1). $H_3Si(OH)AlH_2(OSiH_3)$, BP86/DZPV//VWN/DZPV.
II – $H_3Si(OH)AlH_2(OSiH_3)$, B3LYP/6-31++G**//B3LYP/6-31G* [52].
III – $H_3Si(OH)AlH_2(OSiH_3)$, MP2(fc)/6-31++G**//HF/6-31G* [51].
IV – $H(OH)Al(OH)_3$, MP2(fc)/6-31++G**//HF/6-31G* [51].
V – Collins and O'Malley [54]. $H_3Si(OH)AlH_3$, BLYP/6-31G**.
VI – Rigby et al. [33] $H_3Si(OH)AlH_2(OSiH_3)$, MP2(fc)/6-31G*//HF/3-21G (without symmetry constraints). Reported activation energies (kcal/mol): ethane – 78, propane – 68, n-butane (to CH_4 and C_3H_6) – 67, isobutane – 60. Geometry parameters not reported.
[a] Forming $CH_4 + C_3H_6$.
[b] Forming $C_2H_6 + C_2H_4$.
[c] B3LYP/3-21G(*) values with the $H_3Si(OH)AlH_2(OSiH_3)$ cluster.

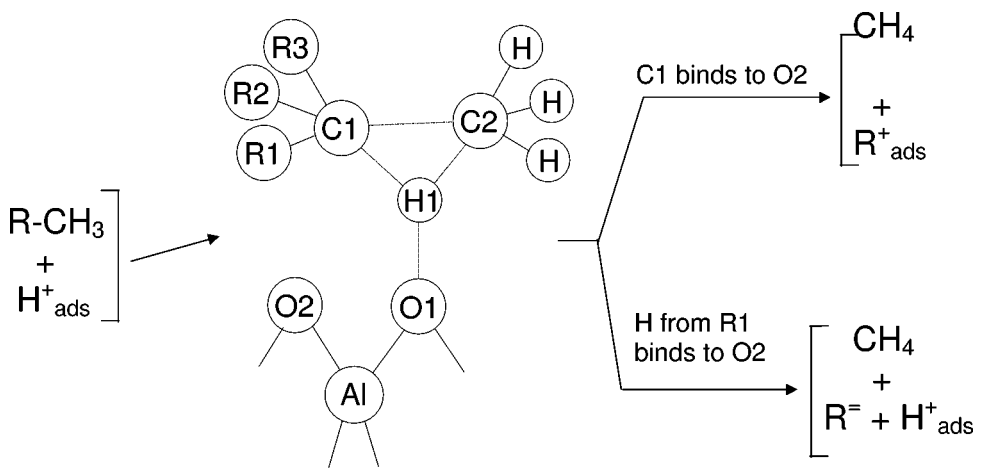

Figure 1. Protolytic cracking of paraffins (schematic).

dicted the s-propyl fragment to react with a zeolite oxygen yielding surface alkoxy. In contrast, calculations of Collins and O'Malley [53,54] and of Rigby et al. [33] for cracking of n-paraffins demonstrated that primary alkyl fragments pass a β-hydrogen atom to a zeolite oxygen yielding directly a regenerated BAS and olefin. The activation energy for isobutane cracking was also computed in the work of Rigby et al. [33] but the products are not reported. Thus the difference in reaction routes may be caused either by the difference in computational methods employed, or by the difference in chemical behavior of primary alkyl fragments formed in cracking of n-paraffins versus the more stable secondary alkyl fragment formed in isobutane cracking [51]. Therefore further calculations are necessary to clarify the issue. In case of ethane protolytic cracking, only the route leading to surface methoxy is possible since olefin with one carbon atom does not exist.

The activation energy for ethane protolytic cracking was computed at various levels. The DFT values are by 4–6 kcal/mol lower than the MP2(fc)/6-31++G**//HF/6-31G* value obtained with the same $H_3Si(OH)AlH_2(OSiH_3)$ cluster. The value for the smaller $H(OH)Al(OH)_3$ cluster is by 4.8 kcal/mol higher since the acid strength of this cluster is lower [51].

The activation energies for protolytic cracking of larger hydrocarbons are calculated to be lower than that for ethane (table 1). According to the results of Rigby et al. [33], the difference between propane and ethane is 10 kcal/mol and between isobutane and ethane – 18 kcal/mol. A slightly larger difference between ethane and isobutane of 22.8 kcal/mol was obtained in our calculations [51]. The activation energy for n-butane cracking forming CH_4 and C_3H_6 is within 1 kcal/mol from the value for propane [33], i.e., addition of extra methyl group to the β-position from the carbenium center has an almost insignificant effect on the activation energy. On the other hand, the difference between the n-butane routes leading to CH_4 and C_3H_6 and to C_2H_6 and C_2H_4 is significant (5.4 kcal/mol) [54]. Collins and O'Malley also used the calculated activation energies and pre-exponential factors to compare the relative rates

of n-butane and n-hexane cracking at different positions [53,54].

3.2. Protolytic dehydrogenation of paraffins

Similar to protolytic cracking, protolytic dehydrogenation of paraffins contributes to catalytic chain initiation. The reaction consists in protolytic cleavage of a C–H bond of paraffin by the zeolite proton. The dihydrogen molecule is released whereas the hydrocarbon residue bounds to a zeolite oxygen. Calculations on protolytic dehydrogenation of methane [8,52,55], ethane [9,51,52,55], propane [52] and isobutane [51] were performed. Their results indicate that the reaction proceeds via a transition state containing a non-classical three-centered bond C(1)–H(2)–H(1), the H(1) hydrogen being still bound to a zeolite oxygen O(1) (see table 2). An example of the transition state for isobutane dehydrogenation is shown in figure 2.

Considering changes of the TS geometry in the sequence CH_4, C_2H_6, C_3H_8, i-C_4H_{10} (table 2, model V), one finds that the O(1)–H(1) bond becomes shorter as the number of methyl groups bound to the carbenium center C(1) increases. The length of this bond drops from 2.025 Å in the TS for CH_4 to 1.667 Å in the TS for i-C_4H_{10}. This is in line with the increase of paraffin proton affinity in this sequence, the saddle point being achieved earlier on the H(1) proton transfer coordinate. The distance from C(1) to hydrogen atoms H(2) and H(1) increases in the sequence, the same happens to the distance from C(1) to the nearest zeolite oxygen. This reflects the increasing stability of the "carbenium-ionic" fragment in the row $CH_3^{\delta+}$, $C_2H_5^{\delta+}$, s-$C_3H_7^{\delta+}$, t-$C_4H_9^{\delta+}$. The particularly large increase of the distance from C(1) to the nearest oxygen when passing from C_3H_8 (2.877 Å) to i-C_4H_{10} (3.990 Å) is also connected with bulkiness of the t-butyl group causing steric hindrances.

The decomposition of the dehydrogenation transition states leads to formation of an H_2 molecule and a surface alkoxy. An alternative reaction route can be suggested, similar to that found for protolytic cracking [53,54] and leading to formation of H_2, olefin and unchanged BAS. An attempt to find such a route for isobutane dehydrogenation was performed [51]. However, the transition state for such a transformation is found to exist only when certain geometry constraints are imposed, and the corresponding activation energy is 7.9 kcal/mol higher than that for the route leading to surface t-butoxy. This indicates that isobutane dehydrogenation with formation of isobutene is unfavorable.

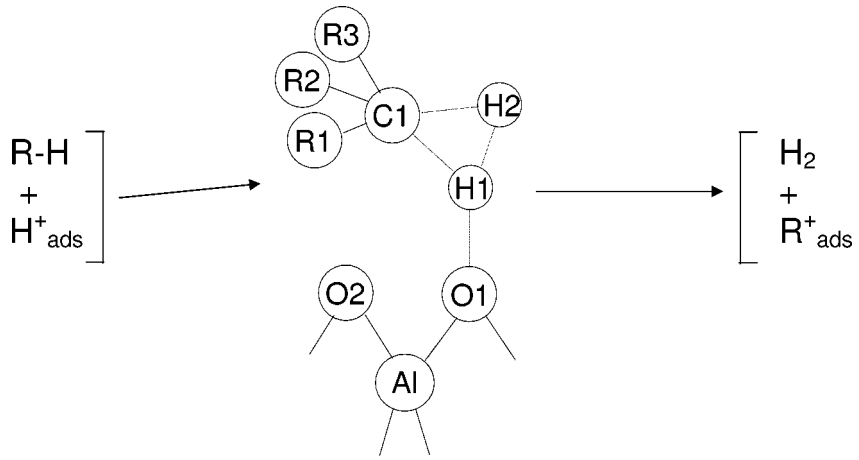

Figure 2. Protolytic dehydrogenation of paraffins (schematic).

Table 2
Protolytic dehydrogenation. Geometry parameters of the transition states in Å, activation energies in kcal/mol.

Model	I	II		III	IV	V			
Paraffin	CH_4	CH_4	C_2H_6	C_2H_6	C_2H_6	CH_4	C_2H_6	C_3H_8	i-C_4H_{10}
C(1)–H(2)	1.666	1.662	1.721	1.778	1.750	1.640	1.715	1.803	1.817
C(1)–H(1)	–	–	–	1.987	1.859	1.704	1.830	2.061	2.216
H(1)–H(2)	0.869	0.915	0.863	0.807	0.760	0.769	0.776	0.775	0.783
O(1)–H(1)	1.590	1.492	1.627	1.762	1.988	2.025	1.823	1.743	1.667
C(1)–$O_{nearest}$	2.118	1.978	2.154	2.397	2.741	2.368	2.519	2.877	3.990
$E^{\#}$	82.0	82.2	71.0	74.7	79.6	95.9	83.9	70.8	66.8

I – Blaszkowski et al. [8] (NLDA-SCF). $H_3Si(OH)AlH_2(OSiH_3)$, BP86/DZPV.
II – Blaszkowski et al. [8,9] (NLDA). $H_3Si(OH)AlH_2(OSiH_3)$, BP86/DZPV//VWN/DZPV.
III – $H_3Si(OH)AlH_2(OSiH_3)$, B3LYP/6-31++G**//B3LYP/6-31G* [52].
IV – $H_3Si(OH)AlH_2(OSiH_3)$, MP2(fc)/6-31++G**//HF/6-31G* [51].
V – $H(OH)Al(OH)_3$, MP2(fc)/6-31++G**//HF/6-31G* [51].

The activation energy decreases when the number of methyl groups bound to the carbenium center C(1) increases (model V in table 2). The decrease is large (12–13 kcal/mol per methyl group) when passing from CH_4 to C_2H_6 and further to C_3H_8. The difference between C_3H_8 and i-C_4H_{10} is much smaller (4 kcal/mol), probably due to bulkiness of the t-butyl group leading to steric hindrances in the TS. The difference in activation energies for CH_4 and C_2H_6 dehydrogenation of 11 kcal/mol found in the DFT calculations of Blaszkowski et al. [8,9] (model II in table 2) is similar to that found in HF calculations (model V). However, the model II activation energies themselves are lower by 13 kcal/mol than the model V values. Approximately 9 kcal/mol of this difference is due to different calculation levels (compare model II and IV values for C_2H_6 obtained with the same cluster), and 4 kcal/mol are due to different clusters used (compare model IV and V values for C_2H_6 obtained at the same calculation level).

3.3. Hydride transfer from paraffins to adsorbed carbenium ions

Hydride transfer is an elementary reaction important for the propagation of the catalytic reaction chain in zeolites. It involves paraffin molecules into chemical transformations by abstracting a hydride anion and forming surface alkoxy groups. The hydride ion is transferred to alkoxy groups earlier formed, releasing paraffins with smaller number of carbon atoms and/or isomerized carbon skeleton. Calculations on methane–methyl [33,40,51,52,56], ethane–ethyl [40,56], propane–s-propyl [33,40,56], propane–t-butyl [40], and isobutane–t-butyl [33,40,51,56] transfers were reported. The activated complexes and/or transition states found for this reaction contain a non-classical three-centered bond C(1)–H(1)–C(2) (see table 3). If no geometry constraints are imposed, the C(1)–Al–C(2) plane is strongly deviated from the O(1)–Al–O(2) plane (dihedral angle varies from 69° to 90° as shown in table 3). It is likely that such an orientation reduces charge separation in the activated complex. An example of the transition state for isobutane–t-butyl hydride transfer is given in figure 3.

The potential energy surface for hydride transfer can contain just one transition state, or two transition states separated by a high-energy local minimum (figure 4). Calculations with the $H(OH)Al(OH)_3$ cluster and full HF/6-31G* geometry optimization [40,56] predicted the methane–methyl and ethane–ethyl transfers to proceed via the latter complex route, whereas the propane–s-propyl, propane–t-butyl, and isobutane–t-butyl transfers to proceed via just one transition state. In contrast, calculations with the $H_3Si(OH)AlH_2(OSiH_3)$ cluster, HF/3-21G geometry optimization and planar symmetry constraints [33] predict all the methane–methyl, propane–s-propyl, and isobutane–t-butyl transfers to proceed via the complex route. The transition states on this complex route are particularly difficult to locate. This was done only for the HF/3-21G methane–methyl transfer route with the cluster $H(OH)Al(OH)_3$ [40,56]. The energy difference between these TS and the high-energy local minimum was found to be 4.8 kcal/mol at the MP2(fc)/6-31++G**//HF/3-21G level. It was suggested that in case of ethane–ethyl transfer this barrier should be even smaller since it disappears fully for propane–s-propyl transfer. Therefore the energy differences between the high-energy local minima and sum of reagent energies were considered as activation energies for methane–methyl and ethane–ethyl hydride transfer.

An alternative reaction route starting with and/or leading to olefins instead of surface alkoxy groups also might be suggested for hydride transfer, similar to that found for protolytic cracking [53,54]. However, such a route has so far not been found in the calculations.

The geometry parameters of the hydride transfer activated complexes exhibit systematic changes when the number of methyl groups bound to carbenium centers increases. The C(1)–C(2) distance increases from 2.142 Å for the methane–methyl complex to 2.584 Å for the isobutane–

Table 3
Hydride transfer. Geometry parameters of the transition states in Å and degrees, activation energies in kcal/mol [a]. MP2(fc)/6-31++G**//HF/6-31G* calculations with the $H(OH)Al(OH)_3$ cluster [40,56].

R1	CH_3	C_2H_5	s-C_3H_7	t-C_4H_9	t-C_4H_9
R2	CH_3	C_2H_5	s-C_3H_7	s-C_3H_7	t-C_4H_9
C(1)–H(1)	1.242	1.253	1.262	1.362	1.292
C(2)–H(1)	1.242	1.253	1.262	1.212	1.292
C(1)–C(2)	2.142	2.331	2.468	2.565	2.584
∠C(1)–H(1)–C(2)	119.2	137.0	156.0	170.4	179.8
∠(O1AlO2) (C1AlC2)	89.7	75.0	75.5	82.2	68.8
C(1)–$O_{nearest}$	2.952	3.026	3.060	3.792	3.809
C(2)–$O_{nearest}$	2.952	3.026	3.060	3.224	3.809
$E^{\#}$	66.6	56.4	47.5	$E^{\#}_{fwd} = 47.3$ $E^{\#}_{rev} = 43.5$	48.4

[a] Activation energies obtained by Rigby [33] et al. with the $H_3Si(OH)AlH_2(OSiH_3)$ cluster at the MP2(fc)/6-31G*//HF/3-21G level with planar symmetry constraints are 80 kcal/mol for methane–methyl and 55 kcal/mol for propane–s-propyl transfer.

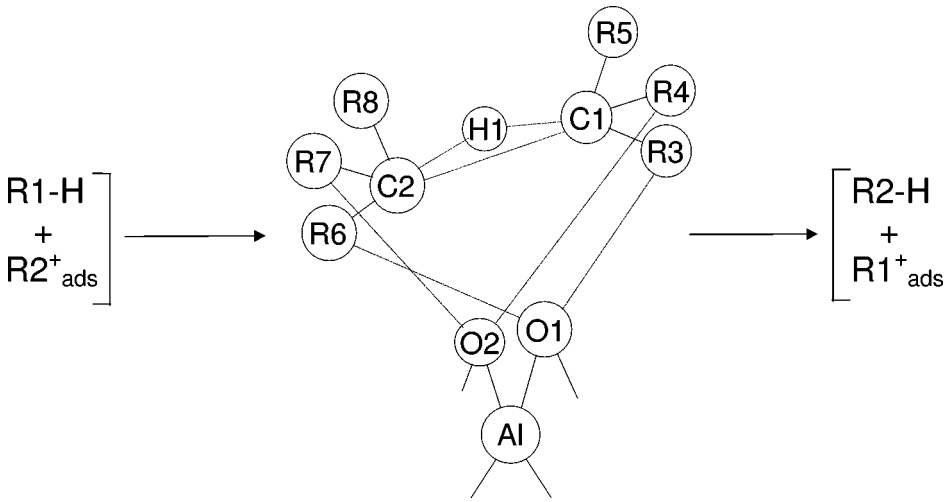

Figure 3. Hydride transfer from paraffins to adsorbed carbenium ions (schematic).

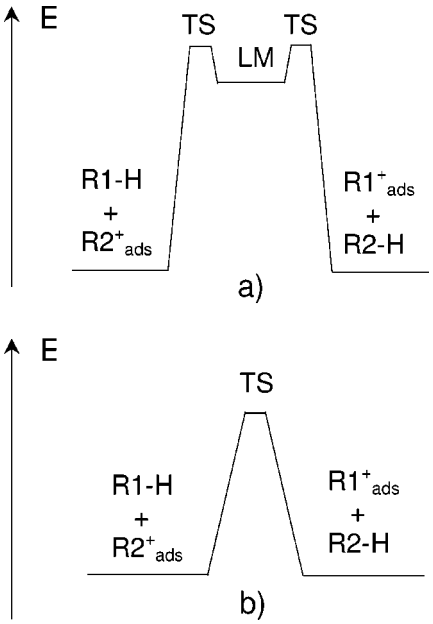

Figure 4. Potential energy profiles for hydride transfer: (a) more complex route with one high-energy local minimum and two transition states found for methane–methyl and ethane–ethyl transfers; (b) more simple route containing just one transition state found for propane–s-propyl, propane–t-butyl, and isobutane–t-butyl transfers.

t-butyl complex, indicating weakening of the bond. The lengths of C(1)–H(1) and C(2)–H(1) bonds increase from 1.242 Å for methane–methyl complex to 1.292 Å for isobutane–t-butyl complex. The bonds in the propane–t-butyl complex are not equal but their average of 1.282 Å also fits the regularity. The C(1)–H(1)–C(2) angle increases in this row from 119.2° to 179.8°. These geometry changes show that the central hydrogen becomes more "hydride" when carbenium-ionic fragments bound to it become more stable. The distance from carbons C(1) and C(2) to the nearest surface oxygen slightly increases in the row CH_3, C_2H_5, s-C_3H_7 as carbenium centers become more stable, and strongly rise for t-C_4H_9 due to bulkiness of this group.

The activation energy decreases with the number of methyl groups surrounding the carbenium centers C(1) and C(2) increases from 0 to 2 (compare methane–methyl, ethane–ethyl, and propane–s-propyl transfers in table 3). The decrease is 4.8 kcal/mol per methyl group on average according to data from [40,56], or 6.3 kcal/mol according to another model [33]. However, the activation energy for isobutane–t-butyl transfer (48.4 kcal/mol) found to be even slightly lower than that for propane–s-propyl transfer (47.5 kcal/mol). Probably this is due to bulkiness of the t-butyl groups causing steric hindrances and overweighing the effect of carbenium centers stabilization by extra methyl groups. The propane–t-butyl transfer activation energy (47.3 kcal/mol) is close to the latter values, whereas the activation energy for the reverse reaction is somewhat lower (43.5 kcal/mol) [40].

The relative energy of the activated complex for methane–methyl transfer with respect to surface methoxy and free methane was computed at several levels with the $H(OH)Al(OH)_3$ and $H_3Si(OH)AlH_2(OSiH_3)$ clusters (table 4). The results obtained indicate that sensitivity of this value to the level of geometry optimization is rather weak (within 1.3 kcal/mol) provided that final energy calculations are performed at the same level. The difference between the MP2(fc)/6-31++G**//HF/6-31G* and B3LYP/6-31++G**//B3LYP/6-31G* values is also small (0.8 kcal/mol). The difference between the values obtained at the same level with different clusters is 6 kcal/mol and is connected with the higher acid strength of the latter cluster.

3.4. Skeletal isomerization of adsorbed carbenium ions

Skeletal isomerization of linear-to-branched paraffins is an important commercial process on its own as branched paraffins have a much higher octane rating [57]. Besides this, skeletal isomerization is an essential elementary step determining the product distribution in other processes such as cracking and alkylation. Isomerization occurs in

Table 4
Activation energies for methane–methyl hydride transfer calculated at various levels (kcal/mol) [40,51,52].

Cluster $H(OH)Al(OH)_3$		Cluster $H_3Si(OH)AlH_2(OSiH_3)$	
MP2(fc)/6-31++G**//HF/3-21G	67.1		
MP2(fc)/6-31++G**//HF/6-31G*	66.6	MP2(fc)/6-31++G**//HF/6-31G*	61.3
MP2(fc)/6-31++G**// MP2(fu)/6-31G*	65.8	B3LYP/6-31++G**//B3LYP/6-31G*	60.5

Table 5
Skeletal isomerization via alkyl shift. Geometry parameters of the transition states in Å, activation energies in kcal/mol. MP2(fc)/6-31G*//HF/3-21G calculations with the $H_3Si(OH)AlH_2(OSiH_3)$ cluster [44]. MS1: propane to propane (carbon scrambling); MS2: n-butane to isobutane; MS3: n-pentane to isopentane (via ethyl shift); MS4: n-pentane to isopentane; MS5: isopentane to isopentane (shift of the existing branch); MS6: 2,3-dimethylbutane to 2,2-dimethylbutane.

	C(1)–C(2)	C(1)–C(3)	C(2)–C(3)	O(1)–C(1)	O(2)–C(2)	$E^{\#}$
			TS type A			
MS1A	1.383	1.921	1.921	2.426	2.426	*65.9*
MS2A	1.382	1.919	1.904	2.683	2.471	*61.6*
MS3A	1.378	1.927	1.927	2.705	2.477	*60.6*
MS4A	1.383	1.914	1.902	2.708	2.472	*60.9*
MS5A	1.383	1.897	1.924	2.769	2.886	54.0
MS6A	1.390	1.892	1.924	3.222	2.727	50.7
			TS type B			
MS1B	1.377	1.899	1.899	2.876	2.876	70.2
MS2B	1.424	1.640	2.237	3.119	2.707	69.5
MS3B	1.405	1.703	2.138	3.183	2.761	63.1
MS4B	1.421	1.648	2.207	3.141	2.715	69.1
MS5B	1.385	1.899	1.899	2.925	2.925	*50.9*
MS6B	1.391	1.945	1.868	3.140	2.904	*46.3*

the adsorbed carbenium ions produced from olefins via chemisorption or from paraffins via hydride transfer, e.g.:

$$n\text{-}C_5H_{12} + R^+_{ads} \rightarrow n\text{-}C_5H^+_{11ads} + R\text{–}H$$
$$n\text{-}C_5H^+_{11ads} \rightarrow \text{(skeletal isomerization)} \rightarrow i\text{-}C_5H^+_{11ads}$$
$$i\text{-}C_5H^+_{11ads} + n\text{-}C_5H_{12} \rightarrow i\text{-}C_5H_{12} + n\text{-}C_5H^+_{11ads} \text{ etc.}$$

Isomerization of n-pentyl and heavier n-alkyl carbenium ions to branched products is believed to proceed via the protonated cyclopropane (PCP) mechanism [58–60] thus avoiding formation of high-energy primary carbenium ions. Movement of the existing branch along the carbon skeleton can proceed without primary ions both via the direct alkyl shift or via the PCP mechanism. Monomolecular isomerization of n-butyl cations can occur via primary carbenium ions only and, therefore, the bimolecular alkylation/cracking route competes with the monomolecular route for n-butane isomerization [57].

Calculations on the direct alkyl shift mechanism [33,44] indicated that this reaction proceeds via a transition state containing a three-membered carbon ring C(1)–C(2)–C(3). Bond distances from C(3) (center of the alkyl group being shifted) to both C(1) and C(2) are longer than a normal single C–C bond, whereas the C(1)–C(2) bond length is between a single and a double bond (see table 5). Two types of transition states (figure 5) for alkyl shift were found when no symmetry constraints were imposed [44]. In the type A TS, the planes O(1)–Al–O(2) and C(1)–C(2)–C(3) are almost parallel; this is very similar to the results obtained with symmetry constraints [33]. In the type B TS, the planes O(1)–Al–O(2) and C(1)–C(2)–C(3) are almost perpendicular, and one or two hydrogen bonds are formed between the oxygen atoms of the cluster and hydrogen atoms bound to the C(1) and C(2) carbons. Distances from the zeolite oxygens to the carbenium centers C(1) and C(2) increase with the number of methyl groups attached to these centers increasing. Indeed, the average of the O(1)–C(1) and O(2)–C(2) distances increases from 2.426 to 2.975 Å for the type A TS, and from 2.876 to 3.022 Å for the type B TS.

The calculated MP2/6-31G*//HF/3-21G activation energies for skeletal isomerization given in table 5 are in the range of 46–66 kcal/mol dependent on the hydrocarbon involved. The value for n-butene-to-i-butene isomerization (61.6 kcal/mol) can be compared to the recently published [45] B3P86/6-31G*, B3P86/6-31G* + ZPE, and MP2/6-31G*//B3P86/6-31G* results: 57.4, 54.4, and 59.1 kcal/mol, respectively. It can be seen that the MP2/6-31G* final energies obtained with different geometry optimization levels are very close, and that the DFT (B3P86) values are somewhat lower than the MP2 values.

Comparison of the calculated activation energies for different hydrocarbons [44] indicates that they decrease by 5.7 kcal/mol on average per each additional methyl group attached to the carbenium centers C(1) and C(2). Effects of the methyl group attached to the C(3) carbon or to the β-position from the carbenium centers are small (within 1 kcal/mol). The difference in activation energies for isomerization of n-butane and n-pentane via the direct alkyl shift is therefore small, whereas a significant difference was

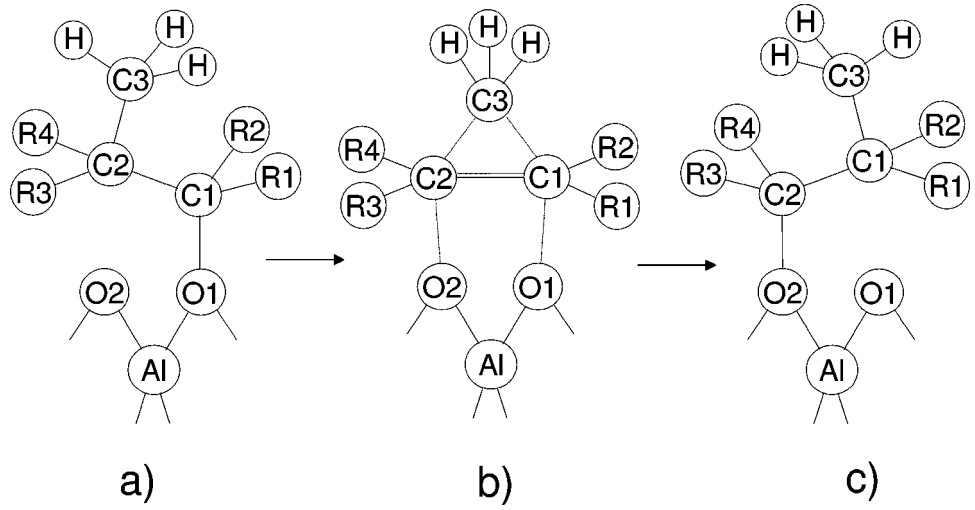

Figure 5. Skeletal isomerization of adsorbed carbenium ions via methyl shift (schematic): (a) initial alkoxy; (b) transition state; (c) final alkoxy.

Table 6
Geometry parameters (in Å) of the free protonated cyclopropane and of the two conformations of the transition state for cyclopropane ring closure. B3LYP/6-31++G**//B3LYP/6-31G* calculations with the $H_3Si(OH)AlH_2(OSiH_3)$ cluster [39].

Structure	C(1)–C(2)	C(1)–C(3)	C(2)–C(3)	C(1)–H(1)	O(1)–H(1)
Free corner-PCP	1.841	1.727	1.393	1.104	–
"Near-in-plane" TS	1.885	1.635	1.415	1.121	2.233
"Out-of-plane" TS	2.148	1.641	1.417	1.096	2.189

found experimentally [59,61,62]. This implies that at least one of these reactions proceeds via the protonated cyclopropane mechanism.

Quantum-chemical calculations on skeletal isomerization of the free (secondary) n-butyl and n-pentyl cations have been performed by Carbo et al. [63] and Boronat et al. [42,64,65]. They found that skeletal isomerization of n-pentyl cation as well as carbon isotope scrambling in n-butyl cation proceeds through the protonated cyclopropanes (1,2-dimethyl- and monomethyl-, respectively). These protonated cyclopropanes represent not local minima but transition states. Skeletal isomerization of n-butyl cation proceeds does not involve protonated cyclopropanes and proceeds via the primary n-butyl cation which also represents a transition state.

In zeolites the reaction route for the PCP skeletal isomerization consists of two steps [33,39,66]. At the first step, the initial alkoxy group is transformed to a substituted cyclopropane. At the second step, the cyclopropane ring is opened in different position yielding an alkoxy group with another carbon skeleton. Calculations on the formation of the *unsubstituted* cyclopropane [33,39] from the surface propoxy provided the transition state geometry for this type of reaction. The hydrocarbon portion of the TS represents protonated cyclopropane whose geometry parameters due to interaction with the cluster are somewhat different from those of the free ion (table 6). The B3LYP/6-31G* calculations predicted two possible orientations of these hydrocarbon portions towards the cluster – "near-in-plane" and

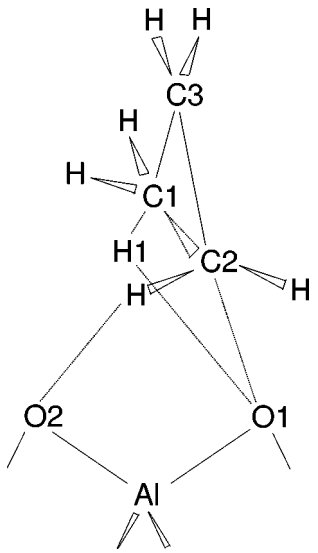

Figure 6. The "out-of-plane" transition state for cyclopropane ring closure.

"out-of-plane", the latter (figure 6) being slightly lower in energy [39]. Only the "out-of-plane" conformation of the TS was located in the HF/3-21G and HF/6-31G* calculations without symmetry constraints [39].

Further calculations on the protonated cyclopropane mechanism of skeletal isomerization [66] provided a comparison of the activation energies for this route with those for the direct methyl shift route. The results obtained indicate that for the n-pentyl-to-isopentyl isomerization the PCP mechanism is much more favorable than the direct

alkyl shift, the activation energy for the former being 13.5 kcal/mol lower than for the latter. Much smaller difference between the two routes for movement of the existing branch in isopentyl was computed, the PCP mechanism being more favorable by 3.2 kcal/mol only. For n-butyl-to-isobutyl isomerization, the PCP route was found to be easier by 7.5 kcal/mol than the direct methyl shift, but more difficult by 6.7 kcal/mol than the PCP isomerization of n-pentyl. The latter value is in a good agreement with the difference of about 6 kcal/mol between the activation energies for n-butane and n-pentane isomerization deduced from the ratio of the experimental rate constants measured on Pt/silica–alumina [59].

3.5. β-scission and alkylation of adsorbed carbenium ions

β-scission is the main elementary reaction responsible for C–C bond cleavage during the chain catalytic cracking process. This reaction occurs in the adsorbed carbenium ions produced from olefins via chemisorption or from paraffins via hydride transfer, e.g.:

$$C_7H_{16} + R^+_{ads} \rightarrow C_7H^+_{15\,ads} + R\text{–}H$$
$$C_7H^+_{15\,ads} \rightarrow (\beta\text{-scission}) \rightarrow C_4H^+_{9\,ads} + C_3H_6$$
$$C_4H^+_{9\,ads} + C_7H_{16} \rightarrow C_4H_{10} + C_7H^+_{15\,ads} \text{ etc.}$$

Calculations of Rigby et al. [33] performed at the MP2(fc)/6-31G*//HF/3-21G level with the $H_3Si(OH)AlH_2(OSiH_3)$ cluster and planar symmetry constraints indicated that the reaction proceeds via a cyclic transition state with three carbons, two oxygens and an aluminium atom in the ring. The activation energies of 71 kcal/mol for the scission of n-butoxy and 60 kcal/mol for 2-methylpent-2-oxy were computed.

Results of Rigby et al. [33] were taken as a starting point for further calculations at the B3LYP/6-31G* and HF/6-31G* levels with the $H(OH)AlH_2(OH)$ and $H_3Si(OH)AlH_2(OSiH_3)$ clusters and without symmetry constraints [41]. Lifting of the symmetry constraints resulted in a significant complication of the potential energy surface. Three reaction routes were identified: route RL – one-step via the "ring-like" transition state (TS); route HBCP – via the "hydrogen-bonded" TS and substituted cyclopropane; and route HB – one-step via the "hydrogen-bonded" TS.

The transition state for route RL (figure 7(a)) is found to be quite similar to that computed with symmetry constraints [33]. However, this route is located only for but-1-oxy β-scission at the B3LYP/6-31G* level with the $H(OH)AlH_2(OH)$ cluster, and has an activation barrier 2.5 kcal/mol higher than that for the HBCP route. Attempts to find the RL transition state for all other combinations of alkoxy, cluster, and geometry optimization procedure were not successful as TS for HBCP or HB routes were obtained instead.

The HBCP route was located with the B3LYP/6-31G* geometry optimization procedure for both but-1-oxy and pent-2-oxy with both the $H(OH)AlH_2(OH)$ and $H_3Si(OH)AlH_2(OSiH_3)$ clusters. The β-scission TS for this route (figure 7(b)) differs from the RL TS primarily by the presence of a hydrogen bond H(1)–O(1). The route includes also a substituted cyclopropane molecule and a TS for its formation from a surface alkoxy. The activation energy for β-scission of pent-2-oxy via this route is found to be lower by around 5 kcal/mol than that for but-1-oxy (table 7).

The HB route was located with the B3LYP/6-31G* geometry optimization procedure for pent-2-oxy with both the $H(OH)AlH_2(OH)$ and $H_3Si(OH)AlH_2(OSiH_3)$ clusters. The β-scission TS for this route is quite similar to the above described HBCP TS, however, the HB route differs from the HBCP one as formation of a substituted cyclopropane does not take place.

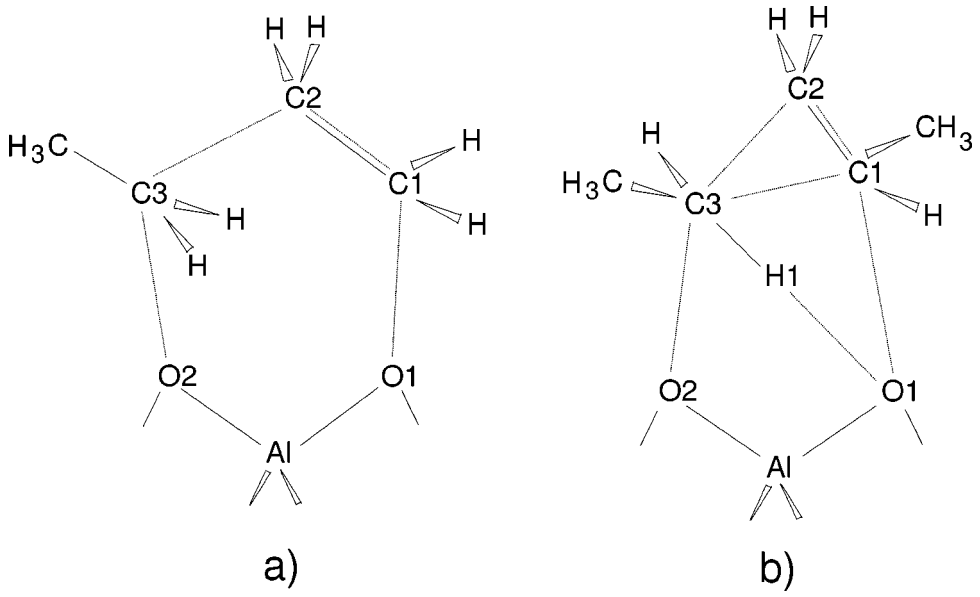

Figure 7. β-scission of adsorbed carbenium ions: (a) but-1-oxy, the "ring-like" transition state; (b) pent-2-oxy, the "hydrogen-bonded" transition state.

Table 7
β-scission. Geometry parameters of the transition states in Å, activation energies in kcal/mol. RL, HBCP, HB – reaction routes. B3LYP and HF mean geometry optimization at the B3LYP/6-31G* and HF/6-31G* levels, respectively. Z_1 = H(OH)AlH_2(OH); Z_2 = H_3Si(OH)AlH_2($OSiH_3$) [41].

Distance	But-1-oxy			Pent-2-oxy			
	RL, Z_1 B3LYP	HBCP, Z_1 B3LYP	HBCP, Z_2 B3LYP	HBCP, Z_1 B3LYP	HBCP, Z_2 B3LYP	HB, Z_1 HF	HB, Z_2 HF
O2–C3	2.341	2.455	2.382	2.427	2.302	2.452	2.427
O1–C1	2.578	3.148	3.359	3.406	3.354	3.335	3.506
C1–C2	1.370	1.359	1.353	1.368	1.358	1.346	1.339
C1–C3	2.638	2.186	2.344	2.375	2.621	2.385	2.600
C2–C3	2.083	2.089	2.311	2.094	2.302	2.203	2.388
$E^{\#}$	66.5	64.0	57.4	59.6	52.4	67.8	64.6

Table 8
Activation energies (in kcal/mol) for β-scission of pent-2-oxy at different levels of the geometry optimization and single point calculations. Z_1 = H(OH)AlH_2(OH); Z_2 = H_3Si(OH)AlH_2($OSiH_3$).

Final energy calculation	Route HBCP (B3LYP/6-31G* optimized)		Route HB (HF/6-31G* optimized)	
	Cluster Z_1	Cluster Z_2	Cluster Z_1	Cluster Z_2
HF/6-31G*	73.3	62.1	71.6	60.1
HF/6-31++G**	69.0	59.6	66.9	57.5
MP2(FC)/6-31G*	72.1	65.0	73.5	66.5
MP2(FC)/6-31++G**	66.9	62.9	67.8	64.6
B3LYP/6-31G*	64.3	54.5	65.3	55.6
B3LYP/6-31++G**	59.6	52.4	60.0	53.3

The dependence of the activation energy on the level of calculations was considered using an example of pent-2-oxy β-scission, since both the B3LYP/6-31G* and HF/6-31G* routes are available for this reaction (table 8). Activation energies found with the $H_3Si(OH)AlH_2(OSiH_3)$ cluster are around 8 kcal/mol lower than those found with the smaller $H(OH)AlH_2OH$ cluster, due to the lower acid strength of the latter cluster. Final energy calculations at the B3LYP level led to values lower by around 7 kcal/mol than those at the HF level, the latter being in turn lower by around 2 kcal/mol than those at the MP2 level. Final energy calculations with the 6-31++G** basis set yielded the activation energy values lower by around 4 kcal/mol than those with the 6-31G* basis set. Geometry optimizations at the B3LYP/6-31G* and HF/6-31G* levels, albeit predicting different reaction paths, led to close (within 2.1 kcal/mol) values provided that final energy calculations are performed at the same level.

Alkylation of surface alkoxy groups with olefins is the reverse of β-scission, therefore it has the same transition state. The activation energy for alkylation is lower than that for β-scission, because formation of olefins from surface alkoxy groups is endoergic while consumption of olefins is exoergic. For instance the calculated at the B3LYP/6-31++G**//B3LYP/6-31G* level with the $H_3Si(OH)AlH_2(OSiH_3)$ cluster enthalpy change for the reaction: $C_2H^+_{5\,ads}$ + H_2C=CH–CH_3 → CH_3–CH_2–CH_2–$(CH_3)CH^+_{ads}$ is −17 kcal/mol, and the corresponding activation energy is 35.4 kcal/mol [41].

3.6. Acid strength variations in the cluster calculations

Variations of acid strength between different zeolites and between different crystallographic sites of the same zeolite are very important for the catalytic properties. To model the acid strength variations in the frame of the cluster approach, Kramer and van Santen [5,6] proposed to change the cluster acid strength by changing lengths of the terminal bonds. Constraining the terminal Si–H bond lengths in the $H_3Si(OH)AlH_2(OSiH_3)$ cluster at values larger than their equilibrium value (about 1.5 Å) enhances the acid strength, and constraining at smaller values reduces the acid strength. Variations of the Si–H distances between 1.3 and 1.7 Å corresponds to the difference in the deprotonation energy of about 20 kcal/mol and this covers the estimated from the force field calculations [67] acid strength range for real zeolites.

This approach was used by Kramer and van Santen [5,6] in calculations of the methane H–D exchange rates on faujasites and zeolites H-ZSM-5. It was found that the activation energy depends only weakly on the overall acid strength of the zeolite, since H–D exchange with methane is a concerted reaction. On the other hand, the *difference* in acid strengths between the initial and final proton (deuteron) position strongly influences the activation energy, the regression obtained from the HF/6-31G** calculations being $E^{\#} = 2.385 + 0.6\Delta(\Delta H_{\mathrm{depr}})$ (energies in eV). This result together with the data on the acid strength values computed for different kinds of sites in faujasites and zeolites H-ZSM-5 allowed to calculate and compare the overall rate constants for these zeolites.

Further calculations of Blaszkowski et al. [9] and Rigby et al. [33] employing the same technique indicated that there are two different classes of elementary steps with respect to their sensitivity to the acid strength variations. Class I consists of the olefin chemisorption, olefin desorption, and the paraffin H–D exchange reactions. Their dependence on the overall acid strength is weak whereas dependence on the acid strength difference between the initial and final proton position is strong. This is because the reactions are concerted and their course depends on the balance between the forming and breaking bonds [5,6]. Class II consists of many reactions including protolytic cracking, protolytic dehydrogenation, hydride transfer, direct alkyl shift, cyclopropane ring opening/closure, and β-scission. Activation energies of these reactions decrease strongly with the overall acid strength increasing. This indicates a more "ionic" nature of the TS for the class II reactions and is correlates with the larger positive charges on the hydrocarbon portions of these TS in comparison with the TS for class I reactions [33]. The activation energy for class II reactions also depends on the acid strength differences and this indicates that even these reactions are not completely "ionic".

Cluster acid strength variations were also used to model the shifts of the zeolite bridging hydroxyl stretching frequency upon adsorption of weak bases [46]. Earlier Paukshtis and Yurchenko [68] proposed a correlation between the logarithm of the shift and the zeolite deprotonation energy: $\log(\Delta\nu_{\mathrm{OH}}) = A + B * \Delta H_{\mathrm{depr}}$. Since the frequency shifts can be relatively easily and accurately measured, the correlation can be used to determine the acid strength of various zeolites. However, both the functional form of the correlation and the numerical values of the constants involved were extrapolated from liquid acids and their experimental testing on zeolites is difficult. Therefore quantum-chemical calculations on the adsorption of ethene, carbon monoxide, and dinitrogen on the zeolite cluster were performed with the cluster acid strength controlled by changing the lengths of the terminal Si–H and Al–H bonds [46]. The results obtained indicated that the dependence of the frequency shift on the zeolite deprotonation energy is indeed accurately logarithmic, and the calculated values of the numerical constants are close to those extrapolated from liquids.

4. Comparison of the calculation results with the experimental data

Experimental measurements of activation energies of elementary steps in hydrocarbon conversion correspond mainly to two elementary steps: protolytic cracking and protolytic dehydrogenation of paraffins. These two reactions can be studied under conditions (high temperature and low conversion) when the accompanying secondary reactions are of minor importance and the final product distribution can be clearly interpreted [1–3]. Three other elementary steps considered here, i.e., hydride tranfer, skeletal

Table 9
Comparison of the calculated and experimental activation energies ($E^{\#}$) for protolytic cracking, protolytic dehydrogenation and hydride transfer for propane, n-butane, and isobutane. Energies in kcal/mol.

Reaction	Hydrocarbon	Zeolite	Experimental $E^{\#}$ (apparent)	Heat of adsorption	Experimental $E^{\#}$ (real)	Calculated $E^{\#}$
Protolytic Cracking	i-C_4H_{10}	FAU	35[a]	10[c]	45	57.5[f]; 60[g]
		H-ZSM5	57[a]	12[d]	69	
		H-ZSM5	31[a]	12[d]	43	
		USY-1	41[a]	(12)[e]	53	
		USY-2	40[a]	(12)[e]	52	
Protolytic cracking	n-C_4H_{10}	H-ZSM5	32–36[a]	12[d]	44–58	60.8[h]; 55.4[h]
		H-ZSM5	33[a]	12[d]	45	67[g]
		H-ZSM5	30[a]	12[d]	42	
		H-ZSM5	32[b]	15[b]	47	
Protolytic cracking	C_3H_8	H-ZSM5	28–33[a]	10[d]	38–43	68[g]
		H-ZSM5	19–22[a]	10[d]	29–32	59[i] (estim.)
		H-ZSM5	34[a]	10[d]	44	
		H-ZSM5	37[b]	10[d]	47	
Protolytic dehydrogenation	i-C_4H_{10}	USY-1	28[a]	(12)[e]	40	66.8[f]
		USY-2	38[a]	(12)[e]	50	
Protolytic dehydrogenation	C_3H_8	H-ZSM5	34[a]	10[d]	44	70.8[i]
Hydride Transfer	i-C_4H_{10}		$<$28–41 (expectation)		$<$40–53	43.5[j] 48.4[j]

[a] [69]. [b] [70]. [c] [74]. [d] [75].
[e] We could not find heats of adsorption on the USY zeolites in the literature, therefore values for silicalite [75] are taken instead.
[f] [51]. [g] [33]. [h] [53]. [i] [52]. [j] [40,56].

isomerization, and β-scission, are usually accompanied by a number of consecutive and parallel reactions. This makes the product distribution more complex and the activation energies more difficult to measure. For hydride transfer from a given paraffin, the activation energy is expected to be somewhat lower than that for protolytic cracking and dehydrogenation of the same paraffin, thus promoting the chain catalytic transformation.

A comparison of the calculated and measured activation energies for several protolytic cracking, protolytic dehydrogenation and hydride transfer reactions is presented in table 9. The experimental activation energies are taken from the review of Jentoft and Gates [69] and from the paper of Narbeshuber et al. [70]. The measured values vary significantly with the reaction conditions, while the computed values vary with the calculation method. The measured apparent activation energies are to be increased by the adsorption heats of the corresponding alkanes, because the surface occupation density decreases with the increase of temperature and this reduces the effect of temperature on the measured reaction rates [70]. Most of the experimental activation energies for protolytic cracking corrected in that way fit the range of 38–53 kcal/mol. Most of the calculated values (except of 67 and 68 kcal/mol obtained with planar symmetry constraints [33]) are in the range of 55–61 kcal/mol, i.e., 2–8 kcal/mol above the upper margin of the experimental values. The corrected experimental activation energies for dehydrogenation are within 40–50 kcal/mol, while the computed values of 67 and 71 kcal/mol are 17–21 kcal/mol higher than the upper margin of the experimental values. The calculated values for hydride transfer from isobutane are within the estimated range of experimental values given in table 9. However, this range is deduced from the experimental data for cracking and dehydrogenation and represents the upper estimate for hydride tranfer. Therefore the computed values for hydride tranfer may be also overestimated by several kcal/mol. Improvement of the agreement between the calculated and the experimental values will require calculations at higher levels and with larger zeolite clusters or periodic structures.

Corrections to the computed activation energies for the cluster acid strength can be obtained from studies of the same reaction as a function of the cluster size [51,71]. Figure 8 shows the corrections for activation energies of protolytic cracking, protolytic dehydrogenation, and hydride transfer reactions found based on the calculated activation

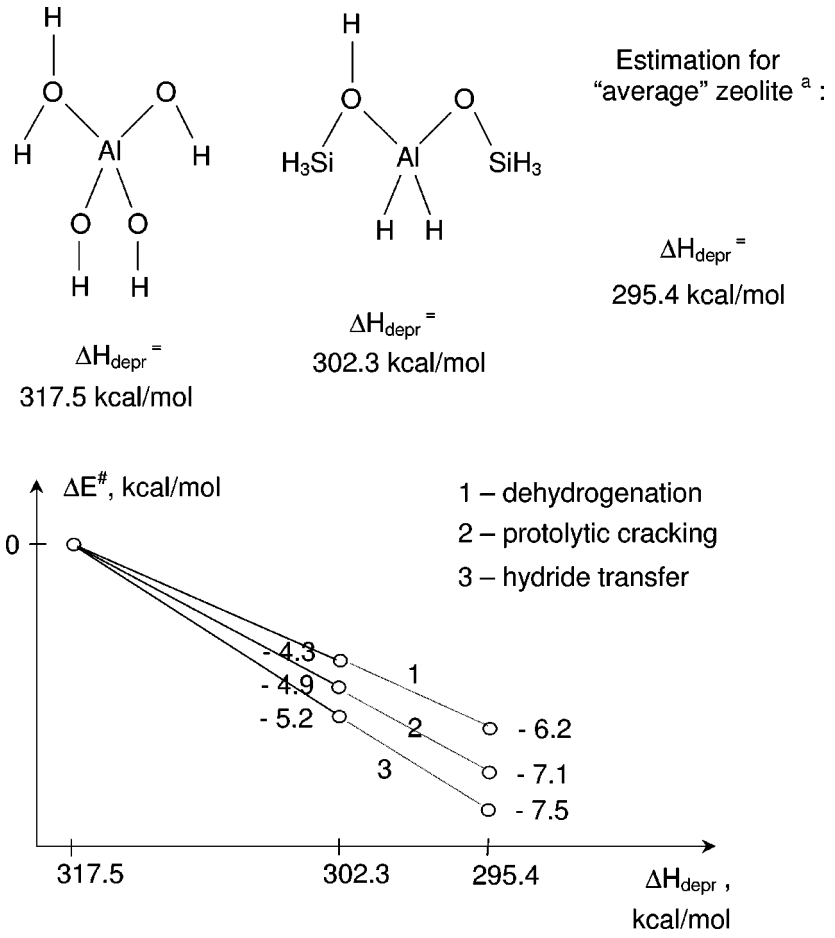

Figure 8. Corrections to the calculated activation energies for the cluster acid strength. Activation energies for protolytic cracking of ethane, protolytic dehydrogenation of ethane, methane–methoxy hydride transfer, and cluster deprotonation energies are computed at the MP2/6-31++G**//HF/6-31G* level with the ZPE corrections. [a]Reference [35].

Table 10
Corrections to the calculated (at the MP2(fc)/6-31++G**//HF/6-31G* level with the $H(OH)Al(OH)_3$ cluster [40,56]) activation energies ($E^{\#}$) for protolytic cracking, protolytic dehydrogenation of and hydride transfer from isobutane. Energies in kcal/mol.

Reaction	Calculated $E^{\#}$	Correction	Corrected $E^{\#}$	Experim. range
Protolytic cracking	57.5	−7.1	50.4	43–53
Protolytic dehydrogenation	66.8	−6.2	60.6	40–50
Hydride transfer	43.5 (to s-C_3)	−7.5	36.0	<40–53
	48.4 (to t-C_4)		41.0	

energies with the (smaller and less acidic) $H(OH)Al(OH)_3$ and the (larger and more acidic) $H_3Si(OH)AlH_2(OSiH_3)$ clusters together with the "average" zeolite deprotonation energy [35]. The linear dependence of the activation energy versus the acid site deprotonation energy is assumed in this plot. The corrections are of the order of 6–8 kcal/mol and are given together with the corrected values in table 10. It can be seen that only the value for dehydrogenation reaction (61 kcal/mol) is still too high even after the correction is applied. The reason for this may be either in computational problems, e.g., basis set size or neglecting of tunneling effects [72], or in the possibility of dehydrogenation on Lewis acid sites [73]. However, the corrected activation energies for protolytic cracking (50 kcal/mol) and hydride tranfer (36 and 41 kcal/mol) are now within the experimental ranges.

5. Conclusion

(1) Results of the quantum-chemical modelling of the of protolytic cracking, protolytic dehydrogenation, hydride transfer, skeletal isomerization, and β-scission reactions show that hydrocarbon portions of their transition states represent carbocations specific for each reaction. Carbonium ions are involved in protolytic cracking and hydride transfer, the hydrogen atom inserted in the C–C bond being connected to a zeolite oxygen in the former and not connected in the latter case. Protolytic dehydrogenation involves H-carbonium ions. Non-classical carbenium ions with three-membered rings of carbon atoms are involved in skeletal isomerization via alkyl shift and via cyclopropane mechanism, and perturbed classical carbenium ions with shortened α and stretched β C–C bonds are involved in β-scission.

(2) Geometry parameters of the TS and activation energies depend on the relative stability of the corresponding carbocations. Increase of the number of methyl groups attached to the carbenium center(s) leads to their stabilization. This causes reduction of the activation energies and in most cases (except of the β-scission reaction) increase of the distances from the carbenium center(s) to the zeolite oxygens. Bulkiness of the t-butyl group causes steric hindrances in the reactions involving t-butyl carbenium center(s), therefore distances from these center(s) to the zeolite oxygens are particularly large and the activation energies are only slightly lower than or close to those for the s-propyl group.

(3) The reactions considered can proceed via several alternative routes dependent on the species involved and on the details of the interaction of the hydrocarbon portion of the activated complex with the zeolite oxygens. The alternatives are: formation of surface alkoxy groups versus formation of olefins in case of protolytic cracking and possibly protolytic dehydrogenation and hydride transfer; direct alkyl shift or the protonated cyclopropane mechanism in case of skeletal isomerization; one-step or cyclopropane-mediated two-step process in case of β-scission.

(4) Variation of the cluster acid strength is a useful technique in quantum-chemical modelling of the acid zeolite catalyzed reactions. It can be employed for studies of the acid strength sensitivity of the activation energies and other quantities of interest as well as for extrapolation of these quantities computed on small clusters towards zeolitic values.

(5) The main limitation of the general use of presented data to the modeling of kinetics in zeolites is the absence of any steric constraints in the reaction intermediates and transition states. The results presented here have to be considered as "ideal" values valid for the situation where these constraints are absent. Future research should focus on techniques to include cavity effects in the calculations [25–32].

References

[1] B.W. Wojcechowski and A. Corma, *Catalytic Cracking: Catalysts, Chemistry and Kinetics* (Dekker, New York, 1986).
[2] I.E. Maxwell and W.H.J. Stork, in: *Introduction to Zeolite Science and Practice*, Vol. 58, eds. H. van Bekkum, E.M. Flanigen and J.C. Jansen (Elsevier, Amsterdam, 1991) ch. 15.
[3] A. Corma, Chem. Rev. 95 (1995) 559.
[4] (a) V.B. Kazansky, Acc. Chem. Res. 24 (1991) 379;
(b) V.B. Kazansky, Stud. Surf. Sci. Catal. 85 (1994) 251.
[5] G.J. Kramer, R.A. van Santen, C.A. Emeis and A.K. Nowak, Nature 363 (1993) 529.
[6] G.J. Kramer and R.A. van Santen, J. Am. Chem. Soc. 117 (1995) 1766.
[7] E.M. Evleth, E. Kassab and L.R. Sierra, J. Phys. Chem. 98 (1994) 1421.
[8] S.R. Blaszkowski, A.P.J. Jansen, M.A.C. Nascimento and R.A. van Santen, J. Phys. Chem. 98 (1994) 12938.
[9] S.R. Blaszkowski, M.A.C. Nascimento and R.A. van Santen, J. Phys. Chem. 100 (1996) 3463.
[10] L.W. Beck, T. Xu, J.B. Nicholas and J.F. Haw, J. Am. Chem. Soc. 117 (1995) 11594.
[11] I.N. Senchenya and V.B. Kazansky, Catal. Lett. 8 (1991) 317.
[12] P. Viruela-Martin, C.M. Zikovich-Wilson and A. Corma, J. Phys. Chem. 97 (1993) 13713.

[13] E.M. Evleth, E. Kassab, H. Jessri, M. Allavena, L. Montero and L.R. Sierra, J. Phys. Chem. 100 (1996) 11368.
[14] S.R. Blaszkowski and R.A. van Santen, J. Am. Chem. Soc. 118 (1996) 5152.
[15] S.R. Blaszkowski and R.A. van Santen, J. Am. Chem. Soc. 119 (1997) 5020.
[16] S.R. Blaszkowski and R.A. van Santen, J. Phys. Chem. B 101 (1997) 2292.
[17] P.E. Sinclair and C.R.A. Catlow, J. Phys. Chem. B 101 (1997) 295.
[18] P.E. Sinclair and C.R.A. Catlow, J. Chem. Soc. Faraday Trans. 93 (1997) 333.
[19] R. Shah, J.D. Gale and M.C. Payne, J. Phys. Chem. B 101 (1997) 4787.
[20] J. Sauer, P. Ugliengo, E. Garrone and V.R. Saunders, Chem. Rev. 94 (1994) 2095.
[21] G.J. Kramer and R.A. van Santen, Chem. Rev. 95 (1995) 637.
[22] S.R. Blaszkowski and R.A. van Santen, Topics in Catal. 4 (1997) 145.
[23] R.A. van Santen, Catal. Today 38 (1997) 377.
[24] J.B. Nicholas, Topics in Catal. 4 (1997) 157.
[25] U. Eichler, C.M. Kölmel and J. Sauer, J. Comput. Chem. 18 (1996) 463.
[26] A.H. de Vries, P. Sherwood, S.J. Collins, A.M. Rigby, M. Rigutto and G.J. Kramer, submitted.
[27] P.E. Sinclair, A. de Vries, P. Sherwood, C.R.A. Catlow and R.A. van Santen, J. Chem. Soc. Faraday Trans. 94 (1998) 3401.
[28] M. Brändle and J. Sauer, J. Molec. Catal. A 119 (1997) 19.
[29] E. Nusterer, P.E. Blöchl and K. Schwarz, Chem. Phys. Lett. 253 (1996) 448.
[30] T. Matsubara, F. Maseras, N. Koga and K. Morokuma, J. Phys. Chem. 100 (1996) 2573.
[31] R.D.J. Froese, S. Humbel, M. Svensson and K. Morokuma, J. Phys. Chem. A 101 (1997) 227.
[32] R. Shah, J.D. Gale and M.C. Payne, J. Phys. Chem. 100 (1996) 11688.
[33] A.M. Rigby, G.J. Kramer and R.A. van Santen, J. Catal. 170 (1997) 1.
[34] F. Haase and J. Sauer, J. Am Chem. Soc. 117 (1995) 3780.
[35] H.V. Brand, L.A. Curtiss and L.E. Iton, J. Phys. Chem. 97 (1993) 12773.
[36] H.V. Brand, L.A. Curtiss and L.E. Iton, J. Phys. Chem. 96 (1992) 7725.
[37] W.J. Hehre, L. Radom, P.v.R. Schleyer and J.A. Pople, *An Initio Molecular Orbital Theory* (Wiley, New York, 1986).
[38] (a) R.G. Parr and W. Yang, *Density-functional Theory of Atoms and Molecules* (Oxford Univ. Press, Oxford, 1989);
(b) J.K. Labanowski and J.W. Andzelm, eds., *Density-functional Methods in Chemistry* (Springer, New York, 1991).
[39] M.V. Frash, V.B. Kazansky, A.M. Rigby and R.A. van Santen, J. Phys. Chem. B 101 (1997) 5346.
[40] V.B. Kazansky, M.V. Frash and R.A. van Santen, Catal. Lett. 48 (1997) 61.
[41] M.V. Frash, V.B. Kazansky, A.M. Rigby and R.A. van Santen, J. Phys. Chem. B 102 (1998) 2232.
[42] M. Boronat, P. Viruela and A. Corma, J. Phys. Chem. 100 (1996) 16514.
[43] S.J. Collins and P.J. O'Malley, Chem. Phys. Lett. 228 (1994) 246.
[44] A.M. Rigby and M.V. Frash, J. Molec. Catal. A 126 (1997) 61.
[45] M. Boronat, P. Viruela and A. Corma, J. Phys. Chem. A 102 (1998) 982.
[46] M.V. Frash, M.A. Makarova and A.M. Rigby, J. Phys. Chem. B 101 (1997) 2116.
[47] (a) H.B. Schlegel, in: *New Theoretical Consepts for Understanding Organic Reactions*, ed. J. Bertran (Kluwer Academic, Dordrecht, 1989) pp. 33–53;
(b) M.J. Frisch, E. Frisch and J.B. Foresman, *Gaussian94 User's Reference* (Gaussian Inc., USA, 1995).
[48] C. Peng, P.Y. Ayala, H.B. Schlegel and M.J. Frisch, J. Comp. Chem. 17 (1996) 49.
[49] C. Gonzalez and H.B. Schlegel, J. Chem. Phys. 90 (1989) 2154.
[50] V.B. Kazansky, I.N. Senchenya, M.V. Frash and R.A. van Santen, Catal. Lett. 27 (1994) 345.
[51] V.B. Kazansky, M.V. Frash and R.A. van Santen, Appl. Catal. A 146 (1996) 225.
[52] V.B. Kazansky, M.V. Frash and R.A. van Santen, unpublished results.
[53] S.J. Collins and P.J. O'Malley, J. Catal. 153 (1995) 94.
[54] S.J. Collins and P.J. O'Malley, Chem. Phys. Lett. 246 (1995) 555.
[55] V.B. Kazansky, M.V. Frash and R.A. van Santen, Catal. Lett. 28 (1994) 211.
[56] V.B. Kazansky, M.V. Frash and R.A. van Santen, Stud. Surf. Sci. Catal. 105 (1997) 2283.
[57] J. Sommer, R. Jost and M. Hachoumy, Catal. Today 38 (1997) 309.
[58] D.M. Brouwer and H. Hogeveen, Progr. Phys. Org. Chem. 9 (1972) 179.
[59] F. Chevalier, M. Guisnet and R. Maurel, in: *Proceedings of the 6th International Congress on Catalysis*, eds. G.C. Bond, P.B. Wells and F.C. Tompkins (The Chemical Society, London, 1977) p. 478.
[60] J. Weitkamp, Ind. Eng. Chem. Prod. Res. Dev. 21 (1982) 550.
[61] G. Zi, C. Jian-min, H. Wei-ming and T. Yi, Stud. Surf. Sci. Catal. 90 (1994) 507.
[62] H. Liu, G.D. Lei and W.M.H. Sachtler, Appl. Catal. A 137 (1996) 167.
[63] S. Carbo, J. Planelles, E. Orti, P. Viruela and F. Tomas, J. Mol. Struct. (THEOCHEM) 150 (1987) 33.
[64] M. Boronat, P. Viruela and A. Corma, J. Phys. Chem. 100 (1996) 633.
[65] M. Boronat, P. Viruela and A. Corma, Appl. Catal. A 146 (1996) 207.
[66] A.M. Rigby and M.V. Frash, unpublished results.
[67] G.J. Kramer and R.A. van Santen, J. Am. Chem. Soc. 115 (1993) 2887.
[68] E.A. Paukshtis and E.N. Yurchenko, Russian Chemical Reviews 52 (1983) 242.
[69] F.C. Jentoft and B.C. Gates, Topics in Catal. 4 (1997) 1.
[70] T.F. Narbeshuber, H. Vinek and J.A. Lercher, J. Catal. 157 (1995) 388.
[71] R.A. van Santen, *Symposiun on Advances and Applications of Computational Chemical Modeling to Heterogeneous catalysis*, Div. Petr. Chem., 213th Meeting, 1997, p. 66.
[72] T.N. Truong, J. Phys. Chem. B 101 (1997) 2750.
[73] A. Corma, P.J. Miguel and A.V. Orchilles, J. Catal. 145 (1994) 171.
[74] F. Eder, M. Stockenhuber and J.A. Lercher, Stud. Surf. Sci. Catal. 97 (1995) 495.
[75] J.R. Hufton and R.P.A. Danner, AIChE J. 39 (1993) 954.